

Possible role of anisotropic membrane inclusions in stability of torocyte red blood cell daughter vesicles

Miha Fošnarič^a, Marjana Nemec^b, Veronika Kralj-Iglič^c,
Henry Hägerstrand^d, Milan Schara^b, Aleš Iglič^{a,*}

^a *Laboratory of Applied Physics, Faculty of Electrical Engineering, University of Ljubljana, Tržaška 25, SI-1000 Ljubljana, Slovenia*

^b *J. Stefan Institute, Ljubljana, Slovenia*

^c *Institute of Biophysics, Faculty of Medicine, University of Ljubljana, Ljubljana, Slovenia*

^d *Department of Biology, Åbo Akademi University, Åbo/Turku, Finland*

Received 23 March 2001; received in revised form 15 October 2001; accepted 2 January 2002

Abstract

The stability of torocyte red blood cell daughter endovesicles induced by octaethylene-glycol dodecylether ($C_{12}E_8$) was studied theoretically. In addition, the effects of $C_{12}E_8$ and tetraethylene-glycol dodecylether ($C_{12}E_4$) on physical properties of the red blood cell membrane were studied experimentally, using the electron spin resonance (ESR) technique. In the theoretical part, it was assumed that the stable vesicle shape corresponds to the minimum of its membrane free energy, which is the sum of the membrane bending energy and the contribution of the $C_{12}E_8$ -induced membrane inclusions. We found that the torocytic vesicle shape may be stable due to quadrupolar ordering of the $C_{12}E_8$ anisotropic inclusions that are embedded in the vesicle membrane. It was also shown how a preference of the membrane inclusions for a specific membrane curvature might lead to their non-homogeneous lateral distribution. In the experimental part, it was shown that $C_{12}E_4$ drastically changes the proportions of the membrane lipid domains (characterized by different 'fluidity'), while $C_{12}E_8$ induces much smaller changes in the proportions of the domains. A possible relation between the difference in the effects of $C_{12}E_8$ and $C_{12}E_4$ on the membrane lipid domains, and their distribution between the membrane leaflets, is discussed. © 2002 Published by Elsevier Science B.V.

Keywords: Red blood cell; $C_{12}E_8$; Non-ionic detergent; Vesiculation; Torocyte shape; Orientational ordering; Electron spin resonance

1. Introduction

We have recently reported [1] that the non-ionic surfactant octaethylene-glycol dodecylether

($C_{12}E_8$) (Fig. 1) may induce in erythrocytes stable torocyte endovesicles having a thin plate-like central region and a toroidal periphery (Fig. 2). It was suggested that the torocyte endovesicle originates from a large stomatocytic invagination of the erythrocyte membrane, which loses volume and finally forms a toroidal endovesicle. Since intercalation of $C_{12}E_8$ into the membrane induces

* Corresponding author. Tel.: +386-1-4250-278; fax: +386-1-4264-630.

E-mail address: ales.iglic@fe.uni-lj.si (A. Iglič).

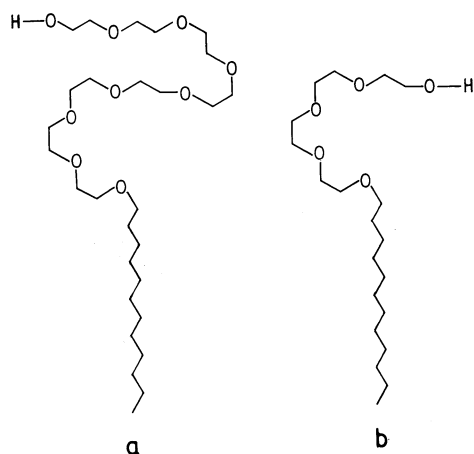


Fig. 1. Schematic illustrations of the chemical structure of octaethylene-glycol dodecylether ($C_{12}E_8$) (A) and of tetraethylene-glycol dodecylether ($C_{12}E_4$) (B).

stomatocytosis (inward membrane bending) and endovesiculation, it was assumed that $C_{12}E_8$ should be located mostly in the inner leaflet of the erythrocyte membrane, i.e. in the outer leaflet of the torocyte endovesicle membrane [1,2].

Although the phase diagram of the stable shapes of the vesicles and the cells with no internal structure has been extensively studied in the past [3–5], aside from a few works [6,2] the torocyte and codocyte shape classes were not given attention. Within the standard bending

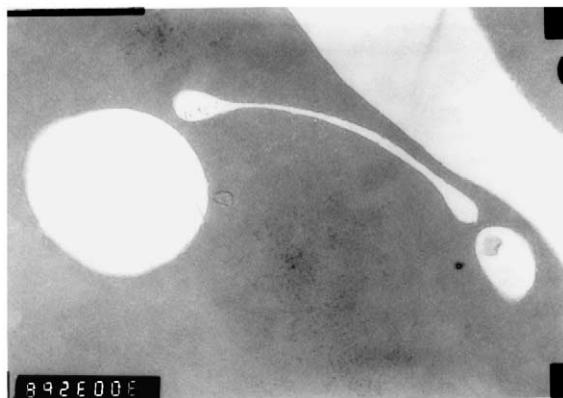


Fig. 2. Transmission electron micrograph of torocyte endovesicles of human red blood cells incubated with $C_{12}E_8$ (adapted from Bobrowska-Hägerstrand et al. [1]).

elasticity models of the bilayer membrane [7,8,4], the calculated torocyte vesicle shapes, corresponding to the minimal bending energy, have a thin central region where the membranes on both sides of the vesicle are in close contact, i.e. the resultant forces on both membranes in contact are balanced [2,6]. However, as it was shown by the confocal laser scanning microscopy [1] and as it can also be seen by the transmission electron microscopy (Fig. 2), the adjacent membranes in the flat central region of the torocyte are separated by a certain distance indicating that the stability of the observed torocyte shapes of the erythrocyte endovesicles can not be explained by the standard bending elasticity model. Therefore it is of interest to understand which additional mechanisms (beside the minimization of the membrane bending energy) might take place in the shape determination of the $C_{12}E_8$ induced torocyte endovesicles.

Three partly complementary mechanisms were suggested in order to explain the formation and stability of the observed torocyte endovesicles [1,2]. The first is a preferential intercalation of the $C_{12}E_8$ molecules into the inner membrane layer, resulting in a membrane invagination that may finally close, forming an inside-out endovesicle. The second mechanism is a preference of the $C_{12}E_8$ induced membrane inclusions (dynamic co-operative units composed of the embedded $C_{12}E_8$ molecule and adjacent membrane constituents that are significantly distorted due to the presence of the embedded $C_{12}E_8$ molecule) for zero or slightly negative [1,2] local mean curvature. Such inclusions would induce the vesicle shape with large regions of zero or slightly negative membrane mean curvatures. The third mechanism is the orientational ordering of anisotropic $C_{12}E_8$ membrane inclusions in the regions of nonzero local membrane curvature deviator [1,2]. The aim of the present work is to investigate the role of these mechanisms in explaining the origin and stability of the torocyte endovesicle shape.

The paper is organized as follows. Materials and methods used in ESR experiments and the

corresponding methods for interpretation of the measured results of ESR experiments are described in Section 2. The expressions for the free energy of the membrane inclusions and for their lateral distribution are derived in Section 3. In Section 4.1, the mathematical model that is used for the theoretical study of the stable torocyte endovesicle shapes is described and the predictions of the model are given. The experimental results from the ESR measurements are reported in Section 4.2. In Section 5, the conclusions are drawn from both experimental and theoretical results. The possible origins of anisotropy of the $C_{12}E_8$ -induced inclusions and of the asymmetric distribution of the $C_{12}E_8$ molecules between both membrane leaflets are discussed. The interdependence between the stable vesicle shape and the non-homogeneous lateral distribution of $C_{12}E_8$ -induced inclusions is also discussed.

2. Materials and methods

2.1. Preparation of erythrocytes and spin labelling of erythrocytes

The cell pellet, 0.2 ml, was dispersed in 6 ml phosphate buffered saline (PBS), transferred into the glass test tube containing 3.0 nmol of the spin probe methyl ester of 5 dioxy palmitate (MeFASL(10,3)) [9] and deposited on the walls. A total of 13.2 ml of PBS for the control or 13.2 ml of PBS containing dissolved C_mE_n was added and all together exposed for 10 min. The sample was centrifuged for 4 min and the pellet was transferred into a glass capillary (inner diameter 1 mm).

2.2. Measurement and simulation of membrane spectra

The electron spin resonance (ESR) spectra were recorded on the Bruker ESP 300 X-band spectrometer at 37 °C. The spectra were recorded at 9.6 GHz microwave frequency and 20 mW power. The modulation frequency and amplitude were 100 kHz and 2.0 gauss. The magnetic scan range was 100 gauss and the scan time was 168 s. The

molar ratio between the membrane spin probe and the phospholipids was about 1/100. The measured spectra of the spin probe in the erythrocyte membrane are superimpositions of spectra of the spin probes dissolved in particular coexisting lateral membrane domains [9,10]. Therefore, the experimental spectra are fitted by the calculated spectra. Three lateral domain types have been assumed. For each type of spectra the corresponding parameters of the spin Hamiltonian function have been selected. The averaged interaction tensor components have been calculated for the properly chosen characteristics of the particular domain, i.e. the molecular ordering of the lipid acyl chains, the rotational correlation times and the polarity corrections due to the alterations of the electronic structure induced by the polarity of the nitroxide environment. The orientation order parameter S describes the alignment of the lipid hydrocarbon chains in the membrane, i.e. a stronger ordering of molecules can be described by higher values of S . Herewith the hyperfine splitting of lines in the spectrum can be directly modified. On the other hand, the line widths depend on the rotational correlation time τ , which reflects the rate of molecular angular deflections of the fluctuating molecular segment, bearing the nitroxide in conformity with the mobility of the neighbouring lipid molecules. The line widths of the spectra are additionally modified by the inherent unresolved hyperfine splitting of the paramagnetic nuclei of the near hydrogen atoms. The polarity corrections due to the membrane regions influence the g and A tensors [11], describing the already mentioned shifts and hyperfine splitting of the spectral lines via the displacement of the unpaired electrons of the nitroxide, that perturbs the wave functions describing the electronic structure of the spin probe.

The optimization of the typical coexisting lateral domains in the proportion set by the population weight parameters and the corresponding line shape parameters was performed for the evaluation of the particular domain's spectra. The program EPR SIM 4.0 was used to solve the described inverse optimization problem. The details are described in Ref. [11].

3. Theory

3.1. Free energy of the membrane inclusions

The anisotropic membrane inclusion in the curvature field of the membrane is considered. It is taken that the inclusion has a C_2 group symmetry with respect to the axis normal to the membrane surface.

Let us imagine that there exists a membrane shape that would perfectly fit the inclusion. This shape is referred to as the membrane shape intrinsic to the inclusion. In general, the local membrane shape at the site of the inclusion differs from the shape intrinsic to the inclusion. The energy of the inclusion is defined as the energy that is spent by adjusting the inclusion into the membrane. Let C_1 and C_2 be the membrane principal curvatures at the site of the inclusion and C_{1m} and C_{2m} the principal curvatures of the shape intrinsic to the inclusion [12]. The energy of a single inclusion can be approximated by the expression [13]:

$$E = \frac{\xi}{2}(\bar{C} - \bar{C}_m)^2 + \frac{\xi + \xi^*}{4}(\hat{C}^2 - 2\hat{C}\hat{C}_m \cos(2\omega) + \hat{C}_m^2) \tag{1}$$

where ξ and ξ^* are the constants representing the strength of the interaction between the inclusion and the surrounding membrane [13,12], $\bar{C} = (C_1 + C_2)/2$, $\hat{C} = (C_1 - C_2)/2$, $\bar{C}_m = (C_{1m} + C_{2m})/2$, $\hat{C}_m = (C_{1m} - C_{2m})/2$ and ω is the angle between the principle directions of the local membrane shape and the corresponding principle directions of the shape intrinsic to the inclusion.

The partition function q of the single inclusion is [14]

$$q = \frac{1}{\omega_0} \int_0^{2\pi} \exp\left(-\frac{E(\omega)}{kT}\right) d\omega \tag{2}$$

where ω_0 is an arbitrary angle quantum, k is the Boltzmann constant and T is the temperature. In the partition function of the inclusion the contribution of the orientational states q_{orient} is distinguished from the contribution of the other states q_c , $q = q_c q_{\text{orient}}$,

$$q_c = \exp\left[\frac{-\xi}{2kT}(\bar{C} - \bar{C}_m)^2 - \frac{\xi + \xi^*}{4kT}(\hat{C}^2 + \hat{C}_m^2)\right] \tag{3}$$

$$q_{\text{orient}} = \frac{1}{\omega_0} \int_0^{2\pi} \exp\left[\frac{\xi + \xi^*}{2kT} \hat{C}\hat{C}_m \cos(2\omega)\right] d\omega \tag{4}$$

The integration over ω yields

$$q_{\text{orient}} = \frac{1}{\omega_0} I_0\left[\frac{\xi + \xi^*}{2kT} \hat{C}\hat{C}_m\right] \tag{5}$$

where I_0 is the modified Bessel function. The free energy of the single inclusion is then obtained by the expression $F_1 = -kT \ln q$,

$$F_1 = \frac{\xi}{2}(\bar{C} - \bar{C}_m)^2 + \frac{\xi + \xi^*}{4}(\hat{C}^2 + \hat{C}_m^2) - kT \ln\left[I_0\left(\frac{\xi + \xi^*}{2kT} \hat{C}\hat{C}_m\right)\right] \tag{6}$$

3.2. Lattice gas model for inclusions embedded in membrane continuum

To obtain the energy contribution of all the inclusions in a membrane layer it is imagined that the membrane layer is divided into patches. The patches are small enough, so that the curvature can be taken as constant over the patch, however they contain enough molecules to be treated by statistical mechanics. The chosen patch can then be considered as a system with well defined principal curvatures C_1 and C_2 , given area A_p , given number of inclusions N_p and given temperature T and is considered to be in local thermodynamic equilibrium.

The inclusions are treated as a two dimensional ideal gas [13,12]. The canonical partition function of the inclusions in a small patch of the membrane layer is $Q = q^{N_p}/N_p!$ [12,13], where q is the partition function of the inclusion and N_p is the number of the inclusions in the patch. Knowing the canonical partition function Q , we can obtain the free energy of the patch, $F_p = -kT \ln Q$. The Stirling approximation is used and the area density of the number of inclusions $n = N_p/A_p$ is introduced. This gives for the area density of the free energy [13].

$$\frac{F_p}{A_p} = -nkT \ln \left[q_c I_0 \left(\frac{\xi + \xi^*}{2kT} \hat{C} \hat{C}_m \right) \right] + kT(n \ln n - n) \tag{7}$$

To obtain the free energy of the inclusions of the whole membrane layer F_L the contributions of all the patches are summed, i.e. the integration over the layer area A is performed $F_L = \int_A (F_p/A_p) dA$, where dA is the area element.

The explicit dependence of the area density n on the position can be determined by the condition for the free energy of all the inclusions to be at its minimum in the thermodynamic equilibrium, $\delta F_L = 0$. It is taken into account that the total number of inclusions N in the layer is fixed,

$$\int_A n dA = N \tag{8}$$

and that the area of the layer A is fixed. The above isoperimetric problem is reduced to the ordinary variational problem by constructing a functional $F_L + \lambda \int_A n dA = \int_A L(n) dA$, where

$$L(n) = -nkT \ln \left[q_c I_0 \left(\frac{\xi + \xi^*}{2kT} \hat{C} \hat{C}_m \right) \right] + kT(n \ln n - n) + \lambda n \tag{9}$$

and λ is the Lagrange multiplier. The variation is performed by solving the Euler equation $\partial L/\partial n = 0$. Deriving Eq. (9) with respect to n and taking into account Eq. (8) gives the Boltzmann distribution function modulated by the modified Bessel function I_0

$$\frac{n}{\bar{n}} = \frac{q_c I_0 \left(\frac{\xi + \xi^*}{2kT} \hat{C} \hat{C}_m \right)}{\frac{1}{A} \int_A q_c I_0 \left(\frac{\xi + \xi^*}{2kT} \hat{C} \hat{C}_m \right) dA} \tag{10}$$

where q_c is given by Eq. (3) and \bar{n} is defined as $\bar{n} = N/A$.

To obtain the equilibrium free energy of the inclusions in the membrane layer the equilibrium density (10) is inserted into the expression (7) and integrated over the area A . Rearranging the terms yields [13]

$$F_L = -NkT \ln \left[\frac{1}{A} \int_A q_c I_0 \left(\frac{\xi + \xi^*}{2kT} \hat{C} \hat{C}_m \right) dA \right] \tag{11}$$

4. Results

4.1. Theoretical predictions

To obtain the equilibrium shape of the vesicle at given area (A) and volume (V), we should minimize the membrane free energy consisting of the contribution of the Canham–Helfrich bending energy and the contribution of the $C_{12}E_8$ induced membrane inclusions in the outer and in the inner membrane bilayer leaflet (F_o and F_i , respectively),

$$F = \frac{1}{2} k_c \int_A (2\bar{C} - C_0)^2 dA + F_i + F_o \tag{12}$$

where k_c is the local bending modulus and C_0 is the spontaneous curvature. In this work it is taken that $C_0 = 0$. The first term in Eq. (12) represents the local bending energy [8]. For the sake of simplicity the non-local bending energy [15–17,4,18] is not considered in Eq. (12). Including the non-local bending energy would not affect the set of possible shapes obtained by the minimization procedure [4,19], since the non-local bending energy does not depend on the details of the shape [20,17].

The contribution of the $C_{12}E_8$ inclusions in the j -th leaflet of the membrane bilayer to the membrane free energy is (see Eq. (11))

$$F_j = -N_j kT \ln \left[\frac{1}{A} \int_A q_{cj} I_0 \left(\frac{\xi + \xi^*}{2kT} \hat{C} \hat{C}_m \right) dA \right] \tag{13}$$

with

$$q_{cj} = \exp \left[\frac{-\xi}{2kT} (\delta_j \bar{C} - \bar{C}_m)^2 - \frac{\xi + \xi^*}{4kT} (\hat{C}^2 + \hat{C}_m^2) \right] \tag{14}$$

where $j = o, i$. The index o denotes the outer leaflet while the index i denotes the inner leaflet of the membrane bilayer, $\delta_i = -1$ and $\delta_o = 1$. N is the total number of the $C_{12}E_8$ inclusions in the j -th leaflet of the vesicle membrane. For the sake of simplicity it is taken in this work that $\xi = \xi^*$.

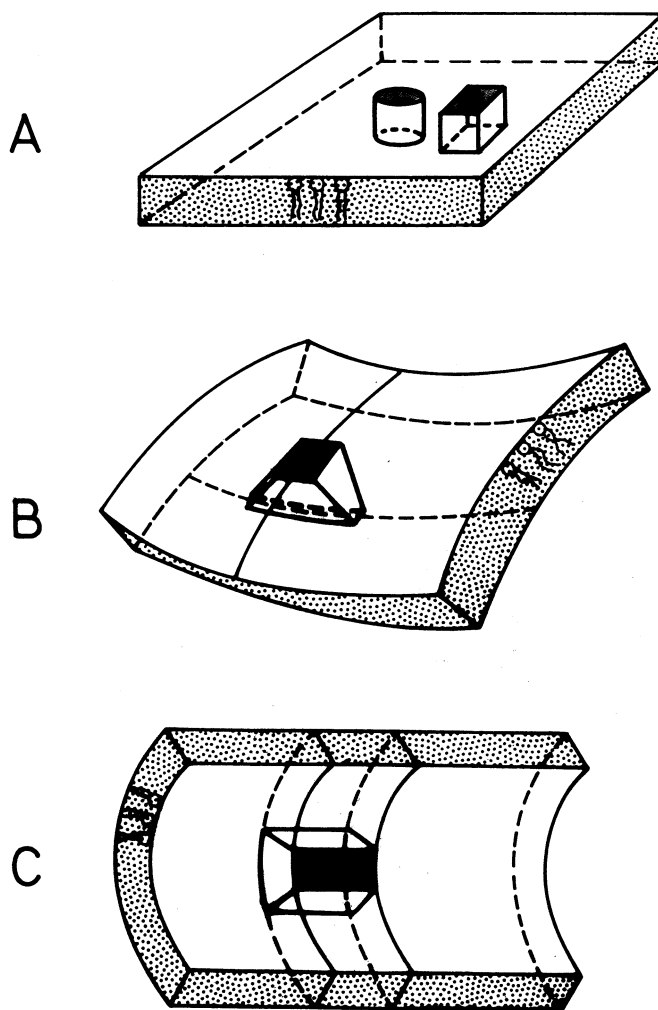


Fig. 3. Schematic figure illustrating different intrinsic shapes of the membrane inclusions characterized by the two intrinsic principal curvatures C_{1m} and C_{2m} . Shading marks the hydrophilic surface of the inclusion. Three characteristic intrinsic shapes of inclusions are shown in the figure: $C_{1m} = C_{2m} = 0$ (A), $C_{1m} > 0$ and $C_{2m} < 0$ (B), $C_{1m} < 0$ and $C_{2m} = 0$ (C). The corresponding most favourable membrane surfaces are also shown.

The integrations in Eqs. (12) and (13) are performed over the entire membrane area A .

In the expression for F_j (Eq. (13)), the quantities $\bar{C}_m = (C_{1m} + C_{2m})/2$ and $\hat{C}_m = (C_{1m} - C_{2m})/2$ contain the information about the effective shape of the inclusions. Here, C_{1m} and C_{2m} are the two intrinsic principal curvatures of the inclusion (Fig. 3). The inclusions are called isotropic if $C_{1m} = C_{2m}$ [20] and anisotropic if $C_{1m} \neq C_{2m}$ [14,12,13] (Fig. 3B and C). The in-plane rotational ordering of the anisotropic inclusions in the curvature field of the

membrane [2] may be strongly coupled to the lateral area density of the membrane inclusions and to the shape of the membrane [12,13,21,14].

In the following, the analysis is restricted to axisymmetric vesicle shapes where the symmetry axis of the vesicle coincides with the y axis, so that the shape is given by the rotation of the function $y(x)$ around the y axis (Fig. 4). In this case the principal curvatures are expressed by $y(x)$ and its derivatives with respect to x as follows,

$$C_1 = -y''(1 + y'^2)^{-3/2} \tag{15}$$

$$C_2 = -y'x^{-1}(1 + y'^2)^{-1/2} \tag{16}$$

where $y' = dy/dx$ and $y'' = d^2y/dx^2$.

The axisymmetric vesicle shape is parametrized by a function of the form

$$y(x) = \left(\alpha + \frac{\gamma^m x^m}{1 + \gamma^m x^m} \right) \sqrt{\beta^2 - x^2} \tag{17}$$

including four free parameters $(\alpha, \beta, \gamma, m)$. In seeking for the minimum of the membrane free energy F , the constraints of fixed vesicle area,

$$A = 4\pi \int_0^\beta x \sqrt{1 + y'^2} dx \tag{18}$$

and volume,

$$V = 4\pi \int_0^\beta xy dx \tag{19}$$

are taken into account.

Dimensionless quantities are introduced (see Appendix A). In the minimization procedure, the parameters α and β , as functions of the parameters γ and m , are determined numerically from the constraints for the vesicle volume (Eq. (19)) and area (Eq. (18)). The remaining parameters γ and m are then determined numerically by the mini-

mization of the relative membrane free energy $f = F/8\pi k_c$ (see Appendix A). The integrals in Eqs. (A1), (18) and (19) are calculated numerically.

Fig. 4 shows the dependence of the calculated equilibrium vesicle shape on the intrinsic principal curvature of the membrane inclusion C_{1m} , for $C_{2m} = 0$. The relative volume is $v = 0.2$ and the values of the parameters are $\kappa = 1$, $\varepsilon_o = 100$ and $\varepsilon_i = 0$ (where $\varepsilon_j \propto N_j T/k_c$ and $\kappa \propto \xi/T$, see Appendix A). The condition $\varepsilon_i = 0$ means that the inclusions are distributed only in the outer leaflet of the membrane bilayer. To illustrate the interdependence between the intrinsic effective shape of the membrane inclusions (determined by C_{1m} and C_{2m}) and the equilibrium vesicle shape (determined by C_1 and C_2), the area density of the membrane inclusions $n_j(x)$ in the j -th membrane leaflet is also calculated (see Eq. (A6)). The area density of the inclusions in the outer layer $n_o(x)$ is shown in Fig. 4 (the value of $n_i(x)$ is zero for all x , since $\varepsilon_i = 0$). It can be seen (Fig. 4a) that the membrane inclusions with zero intrinsic principal curvatures ($C_{1m} = C_{2m} = 0$) favour an oblate shell-like vesicle shape. In this case the vesicle has a large central region of small membrane local mean curvature $\bar{C} = (C_1 + C_2)/2$, where the area density of the inclusions $n_o(x)$ is nearly constant. On the other hand the area density $n_o(x)$ of inclusions with zero intrinsic curvatures is very small at the edge of the vesicle, where the membrane local mean curvature \bar{C} is large and positive.

The central part of the vesicle becomes increasingly thinner and more plate-like while the thickness of the periphery increases with increasing C_{1m} . At $C_{1m} = -3$ (Fig. 4e), the vesicle has a thin plate-like central region and a toroidal periphery and resembles the observed torocytes.

On the basis of the presented results it can be concluded that the calculated equilibrium vesicle shape approaches the shape of the torocyte with increasing the anisotropy of the membrane inclusions that are embedded in the vesicle membrane. The membrane inclusions with zero intrinsic curvatures ($C_{1m} = C_{2m} = 0$) do not favour the torocyte vesicle shape (Fig. 4a).

For the isotropic conical ($C_{1m} = C_{2m} > 0$) and inverted conical ($C_{1m} = C_{2m} < 0$) membrane inclu-

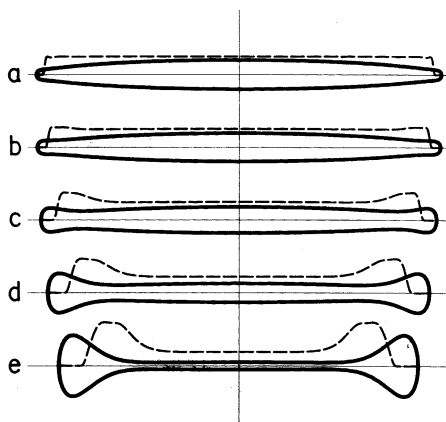


Fig. 4. The calculated equilibrium vesicle shape as a function of the increasing intrinsic principal curvature C_{1m} for $C_{2m} = 0$, $v = 0.2$, $\kappa = 1$, $\varepsilon_o = 100$ and $\varepsilon_i = 0$. The values of C_{1m} are: 0 (a), -1 (b), -2 (c), -2.5 (d) and -3 (e). The corresponding area density of the membrane inclusions in the outer leaflet (n_o) is also shown (broken lines).

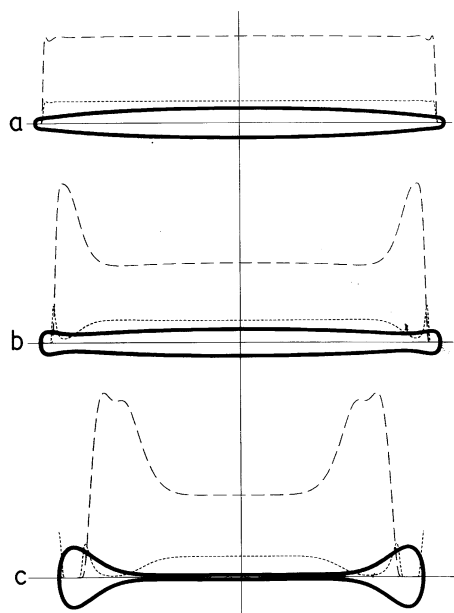


Fig. 5. The calculated equilibrium vesicle shape as a function of the increasing intrinsic principal curvature C_{1m} for $C_{2m} = 0$, $v = 0.2$, $\kappa = 1$, $\varepsilon_o = 80$ and $\varepsilon_i = 20$. The values of C_{1m} are: 0 (a), -2.5 (b) and -2.6 (c). The corresponding area densities of the membrane inclusions in the outer (broken lines) and inner leaflet (dotted lines) of the membrane bilayer are also shown.

sions, the calculated stable torocyte vesicle shapes were not found, neither for the inclusions distributed in the outer leaflet ($\varepsilon_o \neq 0$, $\varepsilon_i = 0$) nor for the inclusions distributed in both leaflets of the membrane bilayer ($\varepsilon_o \neq 0$, $\varepsilon_i \neq 0$).

For comparison, Fig. 5 shows the dependence of the calculated equilibrium vesicle shape on the intrinsic principal curvature of the membrane inclusion C_{1m} for the case where the inclusions are distributed in both leaflets of the membrane bilayer, e.g. $\varepsilon_o = 80$ and $\varepsilon_i = 20$. The values of the other parameters are: $C_{2m} = 0$, $v = 0.2$ and $\kappa = 1$. It can be seen in Fig. 5 that the influence of the intrinsic effective shape of the inclusions on the equilibrium vesicle shape is essentially the same as in Fig. 4. The area density of the inclusions in the outer leaflet $n_o(x)$ (broken lines) differs from the area density of the inclusions in the inner leaflet $n_i(x)$ (dotted line).

4.2. Experimental results

The lateral membrane heterogeneity in terms of co-existing lateral lipid domains with different molecular composition and distinct physical properties has been intensively studied in biological membranes in the last years [22,23,9,10]. In this work, the coexistence of the lateral lipid domains, characterized by different order parameters and rotational correlation times [9,10] was studied using the ESR technique. The ESR experiment shows that the $C_m E_n$ molecules interact with the erythrocyte membrane. We anticipate that the hydrophobic tail of $C_m E_n$ incorporates into the hydrophobic portion of the membrane bilayers. The experimental ESR spectra of the control erythrocytes, as well as the spectra of $C_m E_n$ treated erythrocyte samples have been decomposed into three domain types, where the type I pertains to the most disordered fluid domain, and type III to the most ordered domain. The population proportions of the membrane domains, i.e. the relative weight factors are given in Fig. 6. They have been evaluated using the program EPR SIM 4.0 [11], by which the experimental spectra have been fitted with the calculated spectra for the considering domains. The parameters used are the optimized values of the molecular orientation ordering and molecular dynamics. The obtained parameters and the polarity corrections are shown in Table 1.

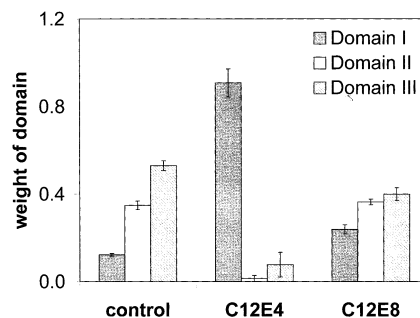


Fig. 6. The lateral domain population of erythrocyte membrane for the control and $C_{12}E_8$ treated samples. The spin probe methyl ester of 5 dioxyl palmitate MeFASL(10,3) was used for EPR measurement. The bars indicate the S.D., referring to five independent experiments. The parameters of domains are given in Table 1.

Table 1
Values of the parameters obtained from the simulation of the experimental ESR spectra for the three types of domains

Parameters	Domains		
	I	II	III
Order parameter S	0.13	0.38	0.73
Rotational correlation time τ (ns)	1.1	0.6	1.0
Additional relax. width (G)	0.7	1.3	2.7
Polarity corrections on A	0.95	0.99	0.99
Polarity corrections on g	1.00015	1.00015	1.0001

Fig. 6 shows that the parameters of the simulation of the experimental ESR spectra of the samples spin-labelled with MeFASL(10,3) changed most strikingly upon binding of $C_{12}E_4$ in the erythrocyte membrane. The effect of $C_{12}E_8$ is smaller. The portion of the most fluid membrane domain I relative to the control membrane is increased in the samples containing $C_{12}E_8$ and also in the samples containing $C_{12}E_4$. However, in the case of $C_{12}E_4$ the increase of the membrane fluidity is drastic.

5. Discussion

In this work the role of $C_{12}E_8$ -induced membrane inclusions in the formation and stability of the torocyte endovesicles was studied theoretically. The equilibrium shape of the vesicle was determined by the minimization of the membrane free energy. A strong coupling between the calculated equilibrium vesicle shape and the lateral distribution of $C_{12}E_8$ -induced inclusions was observed. It was shown that the calculated equilibrium vesicle shapes are torocytic only if the membrane inclusions embedded in the vesicle membrane are anisotropic. In contrast, the isotropic membrane inclusions do not favour the torocyte vesicle shapes. A possible source of anisotropy of the $C_{12}E_8$ membrane inclusions, favouring the torocyte formation, may be the large head group of $C_{12}E_8$ molecule. Another possible reason for the anisotropy of the $C_{12}E_8$ -induced inclusions is that the acyl chains of the phospho-

lipid molecules in the neighbourhood of $C_{12}E_8$ move apart sideways (local phase transition) [24–26]. Based on the described properties of $C_{12}E_8$ molecules and on the $C_{12}E_8$ -phospholipid interactions [27] it has been anticipated that the effective shape of the $C_{12}E_8$ -phospholipid complexes (inclusions) may be anisotropic ($C_{1m} \neq C_{2m}$) [1,2]. In addition, it is known that $C_{12}E_8$ molecules may also interact with membrane proteins and form $C_{12}E_8$ -protein complexes (inclusions) [28]. In general, the effective shape of the $C_{12}E_8$ -protein membrane inclusion may also be anisotropic. Therefore the anisotropic $C_{12}E_8$ -induced membrane inclusions may be $C_{12}E_8$ -phospholipid complexes and/or $C_{12}E_8$ -protein complexes. However in our calculations, the inclusions have been, for the sake of simplicity, considered as equal.

In line with the theoretical predictions given in this work, it was recently suggested that the $C_{12}E_8$ molecules might also stabilize the membrane pores induced by the electroporation [29]. This could be the consequence of an increased area density of the anisotropic $C_{12}E_8$ -induced inclusions at the edge of the pore, favouring highly anisotropic membrane shape at the pore edge.

The effect of $C_{12}E_8$ on the physical properties of the erythrocyte membrane was compared to the effect of $C_{12}E_4$. The $C_{12}E_8$ molecule can be distinguished from the analogous $C_{12}E_4$ molecule as it has a larger hydrophilic head (Fig. 1). The spin probe MeFASL(10,3) [9] may report about the effects of the C_mE_n molecules on the lateral domain distribution (domains I, II and III) at the level of the incorporated nitroxide. The used spin probe is thought to distribute evenly between the inner and the outer leaflet. Fig. 6 shows that $C_{12}E_4$ drastically changes the proportions of the membrane lipid domains relative to the control membrane, while $C_{12}E_8$ induces much smaller changes in the proportions of the domains. This may be partially due to the larger hydrophilic polyethylene head group of the $C_{12}E_8$ molecule that may not be pulled so deep into the membrane as the head group of the $C_{12}E_4$ molecule. Therefore the bound $C_{12}E_8$ induces a different perturbation at the level of the incorporated nitroxide than $C_{12}E_4$. Also, specific interactions between the spin

probe and the C_mE_n molecules cannot be excluded. In addition, the difference between the effects of $C_{12}E_8$ and $C_{12}E_4$ on the ESR spectra may be related to the preferential distribution of $C_{12}E_8$ and $C_{12}E_4$ between the two membrane leaflets. Since $C_{12}E_8$ induces stomatocytic shapes it should be predominantly accumulated in the inner membrane leaflet, while $C_{12}E_4$, which does not markedly affect erythrocyte shape, should be rather evenly distributed between both membrane leaflets [30,31]. A recent report [32] suggests that $C_{12}E_8$ is accumulated in the inner membrane leaflet because the oxyethylene chain binds cations, thereby giving the molecule a positive charge character. The positively charged $C_{12}E_8$ -cation complexes would then be attracted to the negatively charged phospholipids head groups in the inner membrane leaflet. It is also possible that $C_{12}E_8$ is accumulated in the inner membrane leaflet due to polarization interactions [33] directly with the phospholipid head groups in the inner leaflet or with the membrane skeleton.

The presence of C_mE_n molecules in both leaflets requires that C_mE_n molecules can be exchanged between the leaflets. The results from the previous studies indicate a rapid $C_{12}E_8$ transport across the cell membrane [34,35]. The transport of $C_{12}E_8$ from the outer to the inner leaflet of the erythrocyte membrane is also in accordance with the stomatocytogenic effect of $C_{12}E_8$, i.e. the predominant binding of $C_{12}E_8$ in the inner leaflet of the erythrocyte membrane.

Acknowledgements

We are indebted to the Research Institute at the Åbo Akademi University and to the Ministry of Education, Science and Sport of the Republic of Slovenia for their financial support.

Appendix A. Introduction of dimensionless quantities

The unit of length is chosen to be the radius of a spherical vesicle $R_0 = (A/4\pi)^{1/2}$ that has the same area A as the vesicle under consideration.

The variables and parameters are redefined as follows: $x/R_0 \rightarrow x$, $y/R_0 \rightarrow y$, $C_1R_0 \rightarrow C_1$, $C_2R_0 \rightarrow C_2$, $C_{1m}R_0 \rightarrow C_{1m}$, $C_{2m}R_0 \rightarrow C_{2m}$, $\bar{C}R_0 \rightarrow \bar{C}$, $\hat{C}R_0 \rightarrow \hat{C}$, $\bar{C}_mR_0 \rightarrow \bar{C}_m$, $\hat{C}_mR_0 \rightarrow \hat{C}_m$, $\beta/R_0 \rightarrow \beta$, $\gamma/R_0 \rightarrow \gamma$. The volume and the area are normalized relative to the corresponding values of the spherical vesicle with radius R_0 . The relative vesicle volume is $v = (36\pi V^2/A^3)^{1/2}$ and the relative vesicles area is $a = A/4\pi R_0^2 = 1$. The relative membrane free energy $f = F/8\pi k_c$ can be written in terms of normalized quantities as

$$f = \int_a \bar{C}^2 da - \varepsilon_o \psi_o - \varepsilon_i \psi_i \quad (A1)$$

where $j = o, i$,

$$\psi_j = \ln \left[\int_a q_{cj} I_0(\delta_j \kappa \hat{C} \hat{C}_m) da \right] \quad (A2)$$

$$q_{cj} = \exp \left[-\frac{\kappa}{2} ((\delta_j \bar{C} - \bar{C}_m)^2 + \hat{C}^2 + \hat{C}_m^2) \right] \quad (A3)$$

$$\varepsilon_j = N_j kT / 8\pi k_c \quad (A4)$$

$$\kappa = \xi / R_0^2 kT \quad (A5)$$

The expression for the area density of the membrane inclusions $n_j(x)$ in the j -th membrane leaflet is normalized as follows (see Eq. (10)):

$$\frac{n_j(x)}{\bar{n}_j} = \frac{q_{cj} I_0(\kappa \hat{C} \hat{C}_m)}{\int_a q_{cj} I_0(\kappa \hat{C} \hat{C}_m) da} \quad (A6)$$

where $\bar{n}_j = N_j/A$ is the uniform area density.

It was estimated for $R_0 \cong 10 \mu\text{m}$ that the interaction constant κ might be of the order of 10^{-3} [13]. In our case $R_0 \leq 1 \mu\text{m}$, therefore κ may be of the order of 10^{-1} or larger. By taking into account that the area per $C_{12}E_8$ molecule is around 1 nm^2 [36], the area of the torocyte vesicle is $A \cong 5 \mu\text{m}^2$ (Fig. 2), $kT \cong 5 \times 10^{-21} \text{ J}$, $k_c \cong 10^{-19}$ [18] and that the $C_{12}E_8$ molecules occupy around 1% of the leaflet area, we can estimate that $\varepsilon_j \cong 100$.

References

- [1] M. Bobrowska-Hägerstrand, V. Kralj-Iglič, A. Iglič, K. Bialkowska, B. Isomaa, H. Hägerstrand, *Biophys. J.* 77 (1999) 3356.

- [2] A. Iglič, V. Kralj-Iglič, B. Božič, M. Bobrowska-Hägerstrand, B. Isomaa, H. Hägerstrand, *Bioelectrochemistry* 52 (2000) 203–211.
- [3] E. Sackmann, *FEBS Lett.* 346 (1994) 3.
- [4] U. Seifert, *Adv. Phys.* 46 (1997) 13.
- [5] K.H. Parker, C.P. Winlove, *Biophys. J.* 77 (1999) 3096.
- [6] H.J. Deuling, W. Helfrich, *J. Phys. (France)* 37 (1976) 1335.
- [7] P.B. Canham, *J. Theoret. Biol.* 26 (1970) 61.
- [8] W. Helfrich, *Z. Naturforsch.* 28c (1973) 693.
- [9] J. Svetek, B. Kirn, B. Vilhar, M. Schara, *Physiol. Plant.* 105 (1999) 499.
- [10] M. Zuvic-Butorac, P. Müller, T. Pomorski, J. Libera, A. Herrmann, M. Schara, *Eur. Biophys. J.* 28 (1999) 302.
- [11] J. Štrancar, M. Šentjurc, M. Schara, *J. Magn. Reson.* 142 (2000) 254.
- [12] V. Kralj-Iglič, S. Svetina, B. Žekš, *Eur. Biophys. J.* 24 (1996) 311.
- [13] V. Kralj-Iglič, V. Heinrich, S. Svetina, B. Žekš, *Eur. Phys. J. B* 10 (1999) 5.
- [14] J.B. Fournier, *Phys. Rev. Lett.* 76 (1996) 4436.
- [15] E.A. Evans, *Biophys. J.* 16 (1974) 13.
- [16] E. Evans, *Biophys. J.* 30 (1980) 265.
- [17] S. Svetina, A. Iglič, B. Žekš, *Ann. N.Y. Acad. Sci.* 710 (1994) 179.
- [18] W.C. Hwang, R.A. Waugh, *Biophys. J.* 72 (1997) 2669.
- [19] A. Iglič, V. Kralj-Iglič, H. Hägerstrand, *Eur. Biophys. J.* 27 (1998) 335.
- [20] V. Kralj-Iglič, A. Iglič, M. Bobrowska-Hägerstrand, H. Hägerstrand, *Coll. Surf. A* 179 (2001) 57.
- [21] V. Kralj-Iglič, A. Iglič, H. Hägerstrand, P. Peterlin, *Phys. Rev. E* 61 (2000) 4230.
- [22] M. Edidin, *Curr. Opin. Cell. Biol.* 7 (1997) 528.
- [23] K. Simons, E. Ikonen, *Nature* (1997) 569.
- [24] R.L. Thurmond, D. Otten, M.F. Brown, K. Beyer, *J. Phys. Chem.* 98 (1994) 972.
- [25] D. Otten, L. Lobbecke, K. Beyer, *Biophys. J.* 68 (1995) 584.
- [26] H. Heerklotz, H. Binder, G. Lantzsch, G. Klose, A. Blume, *J. Phys. Chem.* (1997) 639.
- [27] H.H. Heerklotz, H. Binder, H. Schmiedel, *J. Phys. Chem. B* 102 (1998) 5363.
- [28] J.V. Møller, M. le Maire, *J. Biol. Chem.* 268 (1993) 18659.
- [29] M. Fošnarič, V. Kralj-Iglič, H. Hägerstrand, A. Iglič, *Cell. Mol. Biol. Lett.* 6 (2001) 171.
- [30] M.P. Sheetz, S.J. Singer, *Proc. Natl. Acad. Sci.* 71 (1974) 4457.
- [31] M.P. Sheetz, S.J. Singer, *J. Cell. Biol.* 70 (1976) 247.
- [32] H. Hägerstrand, J. Bobacka, M. Bobrowska-Hägerstrand, V. Kralj-Iglič, M. Fošnarič, A. Iglič, *Cell. Mol. Biol. Lett.* 6 (2001) 161.
- [33] J. Israelachvili, *Intermolecular and Surface Forces*, Academic Press, New York, 1997.
- [34] U. Kragh-Hansen, M. le Maire, J.V. Møller, *Biophys. J.* 75 (1998) 2932.
- [35] M. le Maire, J.V. Møller, P. Champeil, *Biochemistry* 26 (1987) 4803.
- [36] G. Lantzsch, H. Binder, H. Heerklotz, M. Wendling, G. Krose, *Biophys. Chem.* 58 (1996) 289.